Processing and Application of Ceramics 11 [4] (2017) 247–257
https://doi.org/10.2298/PAC1704247K

Nanocomposite of γ-Fe_2O_3 immobilized on graphene oxide for remediation of Ni(II) ions - Kinetics, isotherm and thermodynamics studies

Manpreet Kaur Ubhi[1], Manpreet Kaur[1,*], Dhanwinder Singh[2], Jean Marc Greneche[3]

[1]*Department of Chemistry, Punjab Agricultural University, Ludhiana-141 004, India*
[2]*Department of Soil Science, Punjab Agricultural University, Ludhiana-141 004, India*
[3]*Institut des Molécules et Matériaux du Mans (IMMM UMR CNRS 6283), Le Mans Université, 72085 Le Mans Cedex 9, France*

Received 8 April 2017; Received in revised form 27 July 2017; Accepted 26 October 2017

Abstract

Facile sonication method was used to immobilize γ-Fe_2O_3 nanoparticles (NPs) on graphene oxide (GO) to obtain environmentally stable γ-Fe_2O_3-GO nanocomposite (NC). Structure, surface morphology and composition of NC were thoroughly studied. Mössbauer analysis confirmed the presence of maghemite (γ-Fe_2O_3) as dominant phase of iron oxide. TEM images of NC revealed homogeneous distribution of γ-Fe_2O_3 NPs over the GO nanosheet. A comparative analysis of GO, γ-Fe_2O_3 NPs and NC for the removal of Ni(II) ions from water was carried out by batch method and adsorption kinetics, thermodynamics and isotherms were also studied. The adsorption data fitted better to Langmuir and Freundlich adsorption isotherms as compared to Dubinin Radushkevich (D-R) and Temkin adsorption isotherms. NC showed higher q_{max} value (615.0 mg/g) as compared to the pristine GO (403.7 mg/g) and γ-Fe_2O_3 NPs (572.4 mg/g). The adsorption kinetics followed pseudo-second-order model. NC displayed greater affinity for Ni(II) ions in comparison to pristine GO and γ-Fe_2O_3 NPs. The results suggested that the synthesized γ-Fe_2O_3-GO nanocomposite can be used as a promising novel material for the removal of Ni(II) from water due to its higher adsorption capacity, stability, convenient magnetic separation and regeneration.

Keywords: *γ-Fe_2O_3, graphene oxide, nanocomposite, structure, adsorption, kinetics, Ni(II) removal*

I. Introduction

The presence of heavy metals in the water is a serious problem of environmental concern. Among heavy metals, Ni(II) is the main pollutant due to its persistence and toxicity which causes various health related problems such as damage of central nervous system, liver dysfunction and cancer [1]. Its concentration varies from 6 to 12 mg/l in the industrial waste water, which is significantly higher than the permissible limit of 3.0 mg/l in industrial effluents [2]. Different techniques viz. electrochemical precipitation, adsorption, electro dialysis, reverse osmosis, co-precipitation, membrane separation, solvent extraction and ion exchange are used for the removal of heavy metal ions [3]. The process of adsorption has received considerable interest as conventional method for the remediation of heavy metals from aqueous solutions due to its simplicity, reversibility via desorption, high efficiency and low operational cost [4,5]. Activated carbon is conventionally used as an adsorbent and synthesis of a new low cost and easily separable adsorbent is an important area of research.

Novel size and shape dependent properties of nanomaterials have been widely explored for the last few decades. Metal oxide nanoparticles (NPs), carbon based nanomaterials and polymeric sorbents are comprehensively used for the removal of heavy metal ions from aqueous solutions [6]. Magnetic iron oxides NPs have excellent physical and chemical properties and are extensively used in catalysis, ceramics, magnetic fluids, data storage and bio applications. They are easy to separate under external magnetic field and have

* Corresponding authors: tel: +91 8146200711,
e-mail: *manpreetchem@pau.edu*

strong adsorption capacity [7]. The different phases of iron oxide NPs are classified as Fe_3O_4 (magnetite), α-Fe_2O_3 (hematite), α-Fe_2O_3 (maghemite) and α-FeOOH (goethite) [8].

Graphene oxide (GO) has a two-dimensional structure, high specific surface area (theoretically ~2600 m^2/g), remarkable chemical stability; it is easily dispersible in water and forms stable suspension. It acts as a good adsorbent material for the treatment of contaminated water [9–13] and shows greater potential of regeneration and reusability over the commercially available adsorbents. GO has been reported as an efficient adsorbent for the removal of dyes [14], pharmaceutical antibiotics [15] and heavy metals [13] but its solubility in water limits its application since separation from the solution after adsorption process is inconvenient. Glycine functionalized GO was used for Ni(II) removal and improvement in adsorption capacity was observed due to the presence of glycine on the surface of GO [16]. Amino siloxane oligomer-linked GO was used as an efficient adsorbent for Pb(II) ions [17]. Aminated GO composite has shown promising adsorption potential for Co(II) ions with adsorption ability of 116.4 mg/g [18]. Novel GO-β-cyclodextrin was synthesized as an adsorbent for the removal of bisphenol-A from solvent phase of aqueous solution [19]. GO-saw dust composite was used as an adsorbent for Ni(II) ions and was subsequently used for the degradation of phenol [20]. Chemical modification of GO with nanomaterials not only makes it water insoluble but also improves its adsorption capacity. Magnetic graphene oxide (MGO) contains Fe_3O_4 and had substantially high adsorption capacity for Cd(II) ions, orange G dye [21], Se(VI) ions [22], Hg(II) ions and methylene blue dye [23]. MGO supported β-cyclodextrin was used as potential adsorbent for Cu(II) ions [24]. Zhang *et al.* [25] have used GO-ferric hydroxide for the removal of As(V) from water. Fe_3O_4-reduced GO composite was also used as adsorbent for As(III)/As(V) and Co(II) removal [26,27]. MGO has low stability under environmental conditions due to oxidation of ferrous (Fe^{2+}) to ferric (Fe^{3+}) phase. MGO is synthesized under nitrogen atmosphere but when used as adsorbent under environmental conditions, the oxidation of nanophase Fe_3O_4 is inevitable. Despite extensive study on the application of MGO as adsorbent for heavy metal ions, no attention has been paid to the issue of stability of MGO. To the best of our knowledge, information pertaining to the application of stable nanocomposite of γ-Fe_2O_3 immobilized on GO as an adsorbent instead of Fe_3O_4-GO composite is lacking.

In the present work, facile sonication method was effectively used to directly immobilize γ-Fe_2O_3 NPs on GO to obtain environmentally stable γ-Fe_2O_3-GO nanocomposite (NC). Structure, surface morphology and composition of the NC were thoroughly studied. The iron oxide phase was characterized by ^{57}Fe Mössbauer spectrometry. The adsorption behaviour of NC for Ni(II) ions was compared with the pristine GO and γ-Fe_2O_3 NPs. Adsorption kinetics was evaluated with pseudo-second order model. The effect of various parameters viz. solution concentration, pH, contact time, temperature and adsorbent dose was quantified and thermodynamic parameters like change in Gibbs free energy ($\Delta G°$), enthalpy ($\Delta H°$) and entropy ($\Delta S°$) were also determined.

II. Experimental

All the chemicals used i.e. graphite powder, sulfuric acid (H_2SO_4), potassium permanganate ($KMnO_4$), sodium nitrate ($NaNO_3$), hydrogen peroxide (H_2O_2), hydrochloric acid (HCl), ferrous ammonium sulfate [$(NH_4)_2Fe(SO_4)_2 \times 6\,H_2O$] ammonium ferric sulfate [$NH_4Fe(SO_4)_2$], potassium persulfate ($K_2S_2O_8$), ammonium hydroxide (NH_4OH), dimethyl glyoxime ($C_4H_8N_2O_2$), nickel chloride hexahydrate ($NiCl_2 \times 6\,H_2O$) were of AR grade. Deionized water was used to prepare the solutions of different strengths.

2.1. Synthesis of γ-Fe_2O_3-GO nanocomposite (NC)

Synthesis pathway for NC is shown in Fig. 1. In the first step, γ-Fe_2O_3 NPs were prepared by dissolving 2.90 g of ferrous ammonium sulfate and 5.35 g ammonium ferric sulfate in 50 ml deionized water. Subsequently, ammonium hydroxide was added into the mixed salt solution until completion of precipitation. The reaction mixture was stirred for 45 min at 80 °C followed by cooling at ambient temperature. γ-Fe_2O_3 NPs were separated from the solution using ordinary magnet then washed with deionized water followed by ethanol and dried at 80 °C for 12 hours in oven.

Graphene oxide (GO) was synthesized by modified Hummer's method [20]. The synthesized GO (1.0 g) and γ-Fe_2O_3 NPs (3.0 g) were separately sonicated in 50 ml deionized water. The solution containing γ-Fe_2O_3 NPs was added slowly to the GO solution during sonication. The mixture was subsequently sonicated for 30 minutes and γ-Fe_2O_3-GO NC was obtained. It was collected using magnet and dried at 60 °C in oven and stored in vacuum desiccator.

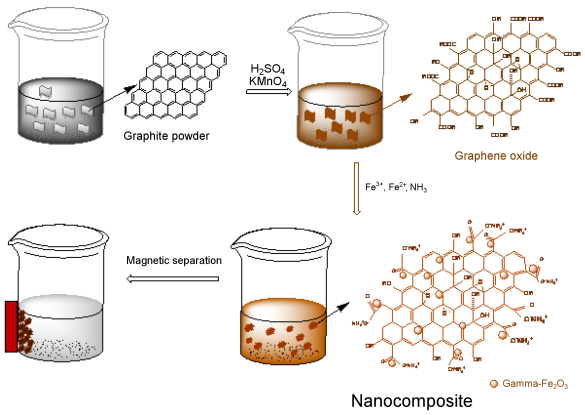

Figure 1. Synthesis of γ-Fe_2O_3-GO nanocomposite (NC)

2.2. Characterization

Techniques viz. X-ray diffraction (XRD), Fourier transform infrared spectroscopy (FT-IR), transmission electron microscope (TEM), scanning electron microscope (SEM-EDS) and vibrating sample magnetometer (VSM) were used as per the standard procedures described by Kaur *et al.* [28]. ^{57}Fe Mössbauer measurements were performed at 300 and 77 K using conventional transmission spectrometer coupled with a constant acceleration drive. The spectra were described by means of magnetic sextets and quadrupolar doublets with Lorentzian lines. The values of isomer shift were quoted with respect to that of α-Fe at 300 K which was also used to calibrate the transducer. The Ni(II) concentration was measured by UV-1800 Shimadzu UV-Visible spectrophotometer.

2.3. Adsorption

The adsorption of Ni(II) ions was studied using batch experiments. Stock solution of Ni(II) ions (1000 mg/l) was prepared by dissolving 4.049 g of $NiCl_2{\times}6\,H_2O$ in 1000 ml of deionized water. Different working solutions of Ni(II) ranging from 50.0–500.0 mg/l were prepared by dilution of stock solution with deionized water. The effect of pH on Ni(II) removal was studied using 100 mg adsorbent with 50 mg/l Ni(II) concentration. The solution pH was adjusted from 2.0 to 10.0 with the addition of 0.5 M HCl and 0.5 M NaOH. The effect of adsorbent dosage (0.01 to 1.0 g) on Ni(II) removal was investigated using initial concentration of Ni(II) 100 mg/l for GO, γ-Fe_2O_3 and NC. The effect of temperature (10 to 40 °C) and contact time on Ni(II) removal was performed using 0.1 g of adsorbent with 100 ml of Ni(II) solution of 100 mg/l concentration. To evaluate the adsorption mechanism, pseudo-second-order kinetic model [29] was applied and is represented as:

$$\frac{t}{q_t} = \frac{K_1 \cdot q_e^2}{2} + \frac{t}{q_e} \tag{1}$$

where q_e and q_t represent amount adsorbed per unit mass at equilibrium and at time t, K_1 is rate constant of pseudo-second-order model. The second order parameters were determined by plotting t/q_t vs. time. The concentration of Ni(II) in the filtrate was determined by dimethyl glyoxime method [30]. All experiments were repeated twice and the mean values were estimated. The adsorption percentage (AP) was determined from the following equations:

$$AP = \frac{C_0 - C_{eq}}{C_0} \cdot 100 \tag{2}$$

where C_0 and C_{eq} are the initial and equilibrium concentrations, respectively. The data were fitted with Langmuir, Freundlich, Temkin and Dubinin-Radushkevich adsorption isotherms. The equations and theoretical parameters are given in Table 1. Thermodynamic parameters i.e. Gibbs free energy change (ΔG°), enthalpy change (ΔH°) and entropy change (ΔS°) were calculated at four different temperature regimes from 10 to 40 °C at the interval of 10 °C using following equations [31]:

$$\Delta G^\circ = -R \cdot T \cdot \ln K \tag{3}$$

where

$$\ln K = -\frac{\Delta H^\circ}{R \cdot T} + \frac{\Delta S^\circ}{R} \tag{4}$$

Table 1. Different adsorption isotherms used and their parameters

Adsorption Isotherms	Equations	Slope	Intercept	Parameters
Langmuir	$\frac{1}{q_e} = -\frac{1}{C_{eq} \cdot b \cdot q_{max}} + \frac{1}{q_{max}}$	$\frac{1}{b \cdot q_{max}}$	$\frac{1}{q_{max}}$	q_{max} is optimum adsorption capacity, C_{eq} is equilibrium concentration, b is energy of adsorption
Freundlich	$\log q_e = \log K_f + \frac{1}{n} \log C_{eq}$	$\frac{1}{n}$	$\log K_f$	q_e is quantity of metal adsorbed per unit weight of adsorbent, n is empirical constant, C_{eq} is equilibrium concentration
Dubinin-Radushkevich	$\ln q_e = \ln q_{max} - \beta \cdot \varepsilon^2$	$-\beta$	$\ln q_{max}$	q_e is amount of metal adsorbed per unit mass of adsorbent, q_{max} is maximum adsorption capacity, β is coefficient associated with energy, $\varepsilon = R \cdot T \ln(1 + 1/C_{eq})$ is polanyi potential, R is universal gas constant, T is temperature, C_{eq} is equilibrium concentration. The mean sorption energy is calculated from the following equation $E = 1/\sqrt{2\beta}$
Temkin	$q_e = B \cdot \ln A + B \cdot \ln C_{eq}$	B	$B \cdot \ln A$	q_e is quantity of metal adsorbed per unit weight of adsorbent, C_{eq} is equilibrium concentration, A is Temkin binding constant, B is heat of adsorption constant

and R is universal gas constant, T is the absolute temperature and K (q_e/C_{eq}) is an equilibrium constant at different temperatures.

III. Results and discussion

3.1. Characterization

It is clearly evident from FT-IR spectrum of GO (Fig. 2a) that oxygen containing functional groups existed in abundance on its surface. It also exhibits characteristic bands for hydroxyl groups (–OH) at 3367 cm^{-1}, carbonyl group (C=O) at 1717 cm^{-1} and C=C at 1609 cm^{-1}. Band at 1220 cm^{-1} is due to the presence of C–O group in the epoxy or phenolic form and band at 1060 cm^{-1} is assigned to C–O group due to the presence of tertiary C–OH group. Wang e*t al.* [32] and Bai *et al.* [33] also noted similar spectrum of GO. FT-IR spectrum of γ-Fe_2O_3 NPs (Fig. 2b) confirms that these were free from organic contaminants and O–H stretching mode of adsorbed water molecules estimated at 3398 cm^{-1} and peak at 1632 cm^{-1} are corresponded to the bending vibrations of –OH group. The bands at 585 and 448 cm^{-1} are assigned to stretching and bending vibrations of the Fe–O bond. FT-IR spectrum (Fig. 2c) of γ-Fe_2O_3-GO (NC) also displays characteristic bands for γ-Fe_2O_3 at 564 and 437 cm^{-1}, assigned to the stretching and bending vibrations of Fe–O bond, respectively [34]. Several peaks with reduced intensity as compared to the pristine GO are observed corresponding to the presence of hydroxyl group (O–H) at 3398 cm^{-1}, C=C stretching at 1622 cm^{-1}, C–O stretching at 1185 cm^{-1} and C–O stretching due to tertiary C–OH group at 1125 cm^{-1}. Disappearance of band at 1717 cm^{-1} might be due to the formation of carboxylate ions. Furthermore, an extra band at 1400 cm^{-1} in NC is assigned to the bending vibrations of nitrogen in NH_4^+ ion. Carboxylate ions reacted with NH_4^+ ions to form $COO^-NH_4^+$ salt. Lewis acid-base interactions were favoured by the presence of iron as it provided binding sites for NH_4^+ ions. Thus, it confirmed that γ-Fe_2O_3 NPs are chemically loaded on GO with the aid of –COOH groups on GO. Huang *et al.* [35] also observed similar phenomenon while studying the effect of surface acidic oxides of activated carbon on the adsorption of ammonia. The presence of NH_4^+ ions in NC was further confirmed by heating the NC with a few drops of NaOH solution in a test tube and colourless gas with typical ammonia-like smell was produced [36]. Analysis of the C : H : N ratio in NC also validated the presence of nitrogen and the ratio was 11.53 : 1.46 : 1.12.

The XRD patterns of graphite, GO, γ-Fe_2O_3 NPs and NC are presented in Fig. 3. Graphite exhibited sharp

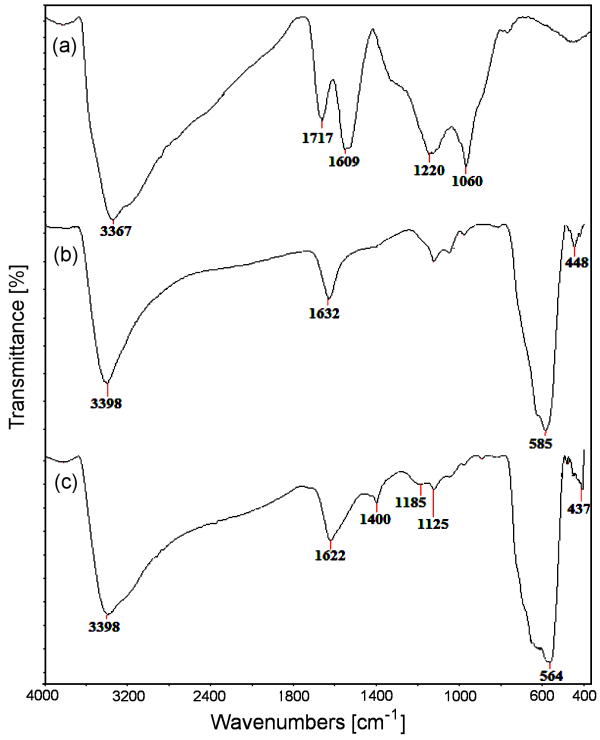

Figure 2. FT-IR spectra of (a) GO, (b) γ-Fe_2O_3 and (c) NC

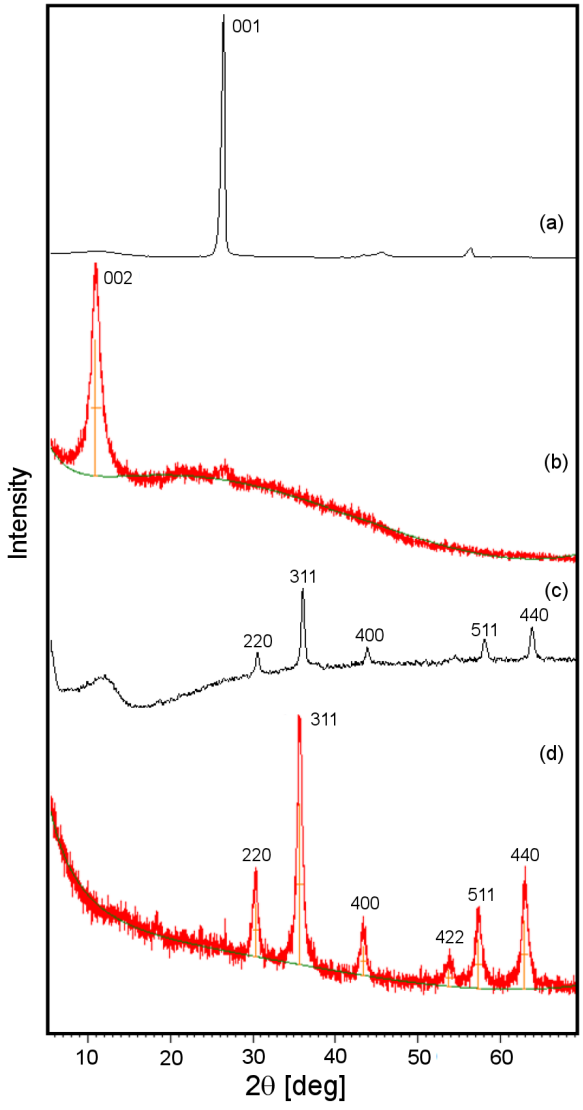

Figure 3. XRD patterns of (a) Graphite, (b) GO, (c) γ-Fe_2O_3 and (d) NC

diffraction peak at $2\theta = 26.5°$ ($d = 0.33$ nm) attributed to the normal graphite spacing of the (001) plane [37]. GO has a characteristic diffraction peak at $2\theta = 10.96°$ ensuing to an interlayer spacing of 0.81 nm and assigned to the (002) plane [13]. Increase in d-spacing from 0.33 to 0.81 nm is related to the oxidation of graphite powder and it further confirmed the presence of oxygen containing functional groups on the surface of GO. XRD patterns of γ-Fe_2O_3 and NC show diffraction peaks at $2\theta = 30.23°$, 35.67°, 43.34°, 53.75°, 57.32° and 62.95° corresponding to the (220), (331), (400), (422), (511) and (440) planes, respectively assigned to maghemite i.e. γ-Fe_2O_3 [38,39]. The broadening of peaks in NC was observed as compared to γ-Fe_2O_3 NPs due to the immobilization of γ-Fe_2O_3 NPs on GO sheets. The absence of GO peak in the XRD of NC might be due to the decrease in aggregation of graphene sheets in the presence of γ-Fe_2O_3 NPs. However, TEM imaging and SEM-EDS established the presence of graphene in the NC. Moreover, the intense signals of γ-Fe_2O_3 over overshadowed the less intense carbon peaks as w/w ratio of GO and γ-Fe_2O_3 was 1 : 3 in the NC. These results are corroborated with the findings of Yang *et al.* [40] who studied the decoration of GO and reduced graphene oxide (RGO) with Fe_3O_4 nanoparticles.

Hysteresis plots (Fig. 4a) depicted the variation in magnetization (M_s) due to the applied magnetic field. The value of saturation magnetization for NC (31.53 emu/g) was lower compared to the γ-Fe_2O_3 NPs (56.86 emu/g) due to the presence of non-magnetic GO. Low coercivity values of 185.9 and 187.0 G for NC and γ-Fe_2O_3 NPs, respectively, also characterized a distinct feature of soft ferrimagnetic material [21].

Mössbauer spectrum of NC measured at 300 K (Fig. 4b down) show broadened magnetic sextet and a central quadrupolar doublet. Isomer shift are identical for the two components and equal to 0.33 mm/s, in fair agreement with the presence of only ferric species. Thus, this excludes the possibility of the presence of mixed Fe^{3+}–Fe^{2+} magnetite phase and confirms that Fe^{2+} phase was fully oxidized into γ-Fe_2O_3 phase i.e. maghemite. At 77 K, the spectrum (Fig. 4b up) consists only of magnetic sextets which can be decomposed into two components, but the small broadening indicates remaining superparamagnetic relaxation phenomena due to ultra-small nanoparticles while the isomer shift values confirm the only presence of Fe^{3+} species.

Scanning electron microscopy analyses confirm layered structure of GO (what is in accordance with the reported SEM images of GO sheets [41]), particle agglomeration of γ-Fe_2O_3 and uniform immobilization of γ-Fe_2O_3 NPs onto the surface of the GO sheets in NC sample. The effective atomic concentrations of carbon and oxygen in GO (determined by SEM-EDS) also confirmed the presence of oxygen containing functional groups on surface as C : O ratio was 0.24 : 1.0. EDS analysis of γ-Fe_2O_3 explained the presence of Fe and O on its surface and the composition of Fe and O ions was

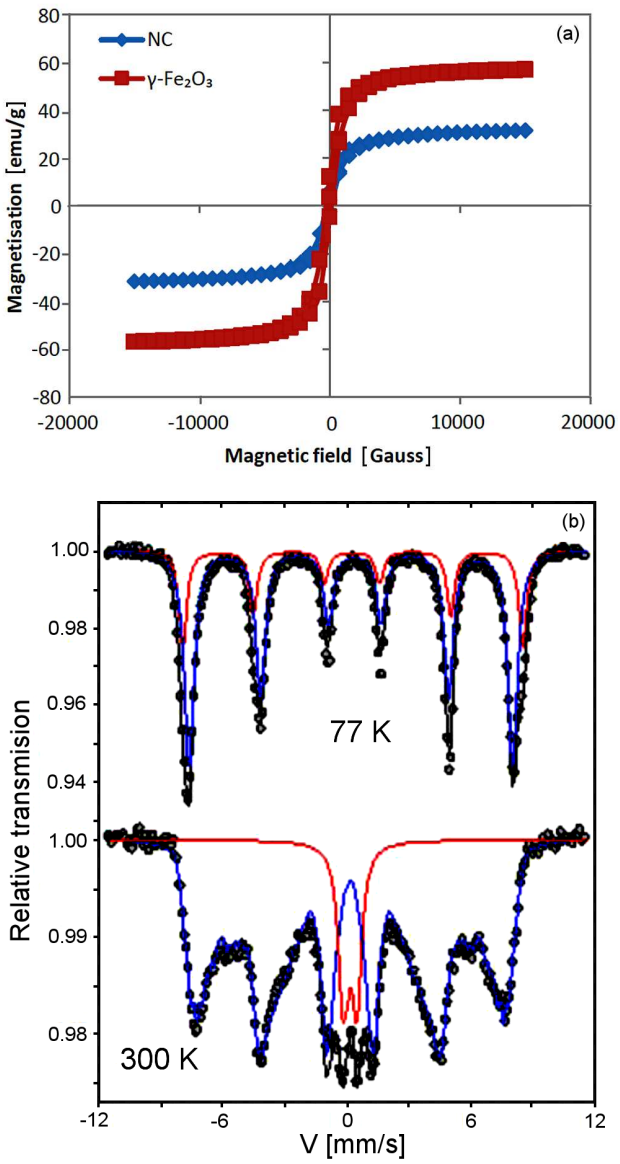

Figure 4. Hysteresis curves of γ-Fe_2O_3 NPs and NC (a) and 300 K and 77 K Mössbauer spectra of NC (b)

80.4% and 19.6%, respectively. The effective atomic concentration of iron, carbon and oxygen on top surface layers of NC was 22.7%, 35.8% and 41.6%, respectively.

TEM micrographs of GO, γ-Fe_2O_3 and NC in aqueous dispersion are presented in Fig. 5. GO nanosheets display several bends and wrinkles due to the functional groups carrying sp^2 hybridized carbon atoms, which were introduced during the oxidation process. GO nanosheets tend to aggregate and formed multilayer agglomerate. γ-Fe_2O_3 NPs are present along with GO nanosheet without damaging the layered structures as observed in TEM of NC (Fig. 5c). Hur *et al.* [42] reported similar trend for Fe_3O_4 loaded on GO in different proportions. The selected area in Fig. 5c revealed the uniform spherical homogeneous distribution of γ-Fe_2O_3 NPs over the GO nanosheet.

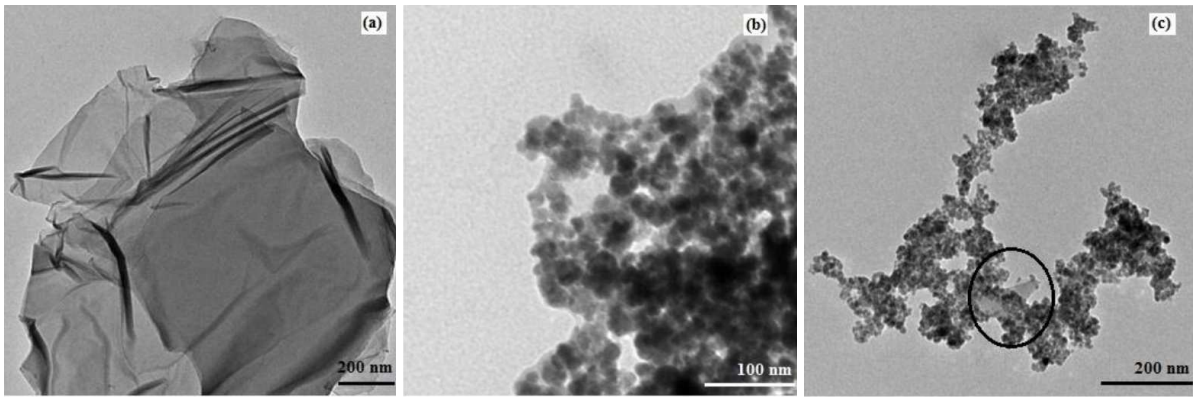

Figure 5. Transmission electron micrographs of: a) GO, b) γ-Fe_2O_3 and c) NC

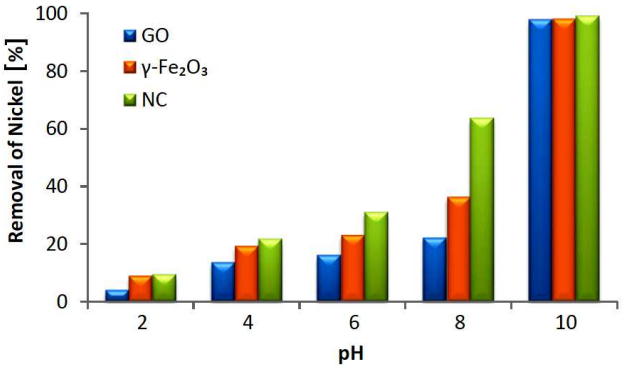

Figure 6. Effect of pH on Ni(II) ions removal at 25 °C using GO, γ-Fe_2O_3 and NC

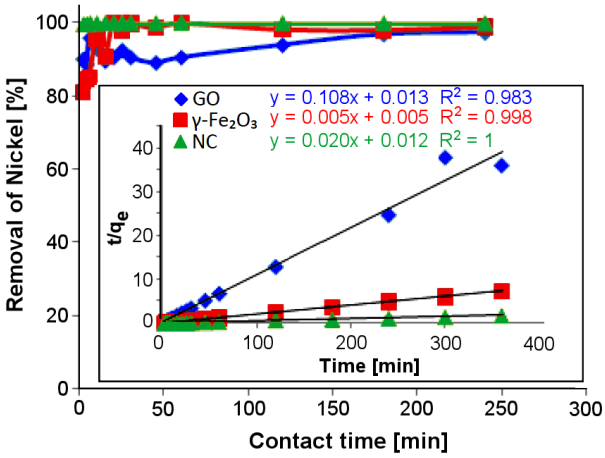

Figure 7. Effect of contact time on Ni(II) removal (inset - plot of t/q_e vs time (pseudo-second order model) for Ni(II) ions adsorption at 25 °C using GO, γ-Fe_2O_3 and NC)

3.2. *Effect of pH*

The adsorption of Ni(II) ions at the solid-water interface is strongly influenced by the solution pH (Fig. 6). Adsorption capacity of GO, γ-Fe_2O_3 and NC is lower at low pH due to the competition between the excess of H_3O^+ ions and Ni(II) ions for the sorption sites. The number of negatively charged sites on the adsorbent surface increased at higher solution pH, which in turn assisted the adsorption of positively charged Ni(II) ions. At solution pH = 6, removal of Ni(II) ions was 16.0%, 23.0% and 31.0% for GO, γ-Fe_2O_3 and NC, respectively. Simultaneous adsorption and precipitation were observed at pH = 10.0 and removal was 98.1%, 98.3% and 99.3% for GO, γ-Fe_2O_3 and NC, respectively. Similar trend was also observed by Patil *et al.* [43] while studying the adsorption of Ni(II) onto activated carbon.

3.3. *Adsorption kinetics*

Adsorption capacity increased sharply with time and equilibrium was attained within 15 min, 2 h and 20 min for GO, γ-Fe_2O_3 and NC, respectively (Fig. 7). Ni(II) removal from the synthetic solution was significantly faster during the initial phase as a large number of vacant sites were available for the adsorption. With the increase in contact time, the unoccupied sites were gradually difficult to occupy due to the repulsive forces between Ni(II) ions on the solid and in the solution. Plot of t/q_e versus t (inset of Fig. 7) and correlation coefficient (R^2) >0.98 signified that the adsorption of Ni(II) ions was linearly correlated with pseudo-second-order model. The calculated values of q_e were comparable with the observed values (Table 2).

Table 2. Parameters of pseudo second-order kinetic model for different adsorbents

Adsorbent	q_e [mg g^{-1}]	Rate constant, k_1 [g mg^{-1}min^{-1}]	R^2
GO	99.3	3.03×10^{-4}	0.98
γ-Fe_2O_3	98.0	8.85×10^{-3}	0.99
NC	98.3	9.6×10^{-6}	1.00

3.4. *Effect of adsorbent dose*

It is clear from Fig. 8 that removal of Ni(II) up to the 99.2% and 98.8% was achieved with the use of 0.01 g NC and γ-Fe_2O_3 NPs as absorbents, respectively. On the increasing adsorbent dose decrease in Ni(II) removal from the solution was observed for γ-Fe_2O_3 NPs and NC. However the decrease was more pronounced for the NC. VSM analysis also supported the present findings as magnetization value of γ-Fe_2O_3 (56.86 emu/g) was higher than NC (31.52 emu/g). Higher magnetiza-

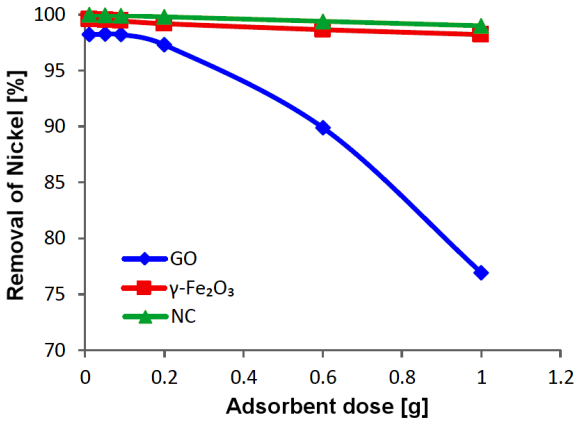

Figure 8. Effect of adsorbent dose on Ni(II) ions adsorption at 25 °C using GO, γ-Fe_2O_3 and NC

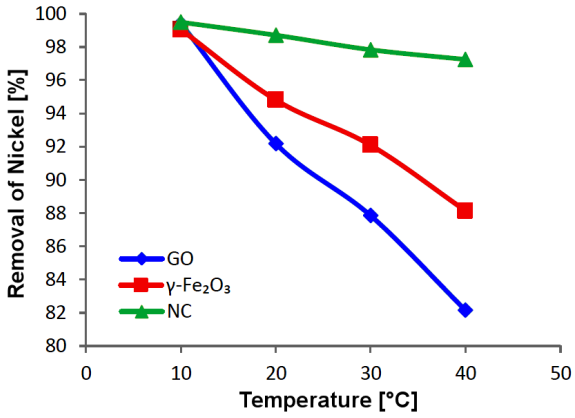

Figure 9. Effect of temperature on Ni(II) ions adsorption using GO, γ-Fe_2O_3 and NC

tion caused greater agglomeration of γ-Fe_2O_3 and decreased the available surface area of NPs. Whereas, the removal of Ni(II) ions decreased appreciably with an increase in the adsorbent dose of GO. The Ni(II) removal decreased from 98.0% to 77.0% as the dose of adsorbent was increased from 0.01 to 0.1 g. At higher GO concentration, interactions between GO flakes physically hindered the binding sites from adsorbing Ni(II) ions from aqueous solution. Attractive force between Ni(II) ions and the surface of individual GO nanosheet was reduced further due to the creation of electrostatic interferences [29].

3.5. *Thermodynamic analysis*

The adsorption capacity of synthesized GO, γ-Fe_2O_3 NPs and NC was studied in the temperature range of 10 to 40 °C. At higher temperature, Ni(II) removal capacity of all three adsorbents was decreased (Fig. 9). At 10 °C maximum removal of Ni(II) ions was 99.4%, 99.0% and 99.4% and at 40 °C it was 82.1%, 88.1% and 97.2% for GO, γ-Fe_2O_3 NPs and NC, respectively. This signifies that adsorption was exothermic which is too supported by $\Delta H°$ values of −0.04, −0.05 and −0.03 kJ/mol for GO, γ-Fe_2O_3 NPs and NC, respectively. Thermodynamic parameters were calculated from the adsorption studies performed at four different temperatures (10–40 °C). The values of $\Delta H°$ and $\Delta S°$ were calculated from the slope and interception of the plot of $\ln K$ vs. $1/T$ (Fig. 10) and presented in Table 3. The value of $\Delta G°$ up to −20 kJ/mol indicates the existence of electrostatic interactions between active sites and Ni(II) ion (physisorption); value less than −40 kJ/mol signifies charge sharing or transfer from the adsorbent to Ni(II)

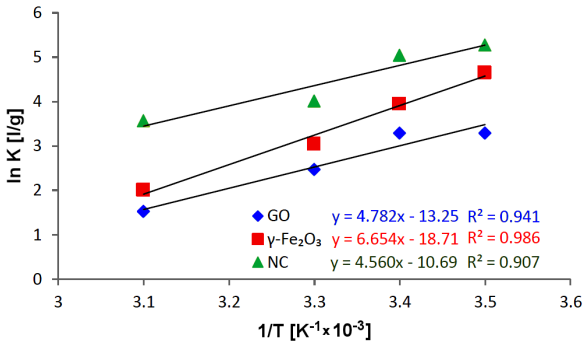

Figure 10. Plot of $\ln K$ vs $1/T$ to predict thermodynamic parameters for the adsorption of Ni(II) ions onto GO, γ-Fe_2O_3 and NC

ion to form a dative bond which depicts chemisorption [44]. The $\Delta G°$ values obtained in the present studies were less than −13 kJ/mol indicated that physical adsorption was the predominant mechanism in the sorption process. The negative value of $\Delta G°$ decreased from −7.75 to −3.97, −10.94 to −5.22 and −12.42 to −9.28 kJ/mol as temperature raised from 10 to 40 °C for GO, γ-Fe_2O_3 NPs and NC, respectively. This confirmed spontaneous nature of adsorption being more favourable at low temperature. $\Delta S°$ values of −0.11, −0.14 and −0.08 kJ/mol K for GO, γ-Fe_2O_3 NPs and NC suggested that degree of freedom of the adsorbed species was decreased [45].

3.6. *Effect of Ni(II) ion concentration*

The percentage removal was decreased with the increase in Ni(II) concentration in the solution (Fig. 11). At 50 mg/l Ni(II) solution, the removal of 99.0%, 99.6%

Table 3. Thermodynamic parameters for the adsorption of Ni(II) ions onto GO, MO NPs and NC

Sample	$\Delta H°$	$\Delta S°$	$\Delta G°$ [kJ/mol]				R^2
	[kJ/mol]	[kJ/mol/K]	283	293	303	313	
GO	−0.04	−0.11	−7.75	−8.02	−6.21	−3.97	0.94
γ-Fe_2O_3	−0.05	−0.14	−10.94	−7.41	−7.43	−5.22	0.98
NC	−0.03	−0.08	−12.42	−10.60	−9.60	−9.28	0.90

Table 4. Estimated Langmuir, Freundlich, D-R and Temkin parameters for Ni(II) adsorption

Adsorbent	Langmuir			Freundlich			D-R				Temkin			
	q_{max}	$b \times 10^{-2}$	R^2	n	K_f	R^2	q_{max}	$\beta \times 10^{-6}$	E	R^2	A	B	b	R^2
GO	403.7	4.2	0.94	1.27	16.8	0.96	250.2	3.0	0.40	0.59	0.11	208.0	11.9	0.89
γ-Fe_2O_3	572.4	5.9	0.98	1.67	41.9	0.97	302.7	2.0	0.50	0.86	0.63	112.2	22.1	0.94
NC	615.0	3.9	0.99	1.77	49.5	0.98	293.1	1.0	0.70	0.82	0.80	107.6	23.0	0.96

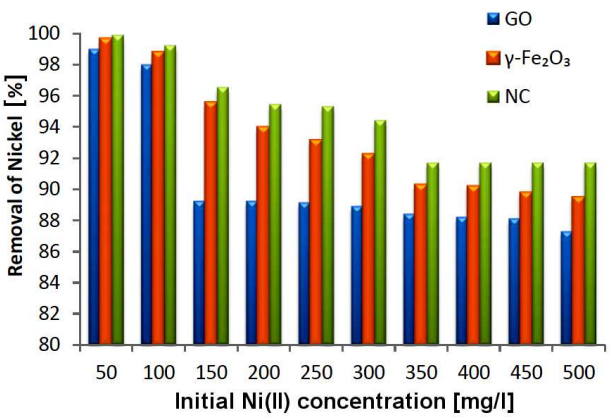

Figure 11. Effect of initial concentration on Ni(II) ions adsorption at 25 °C using GO, γ-Fe_2O_3 and NC

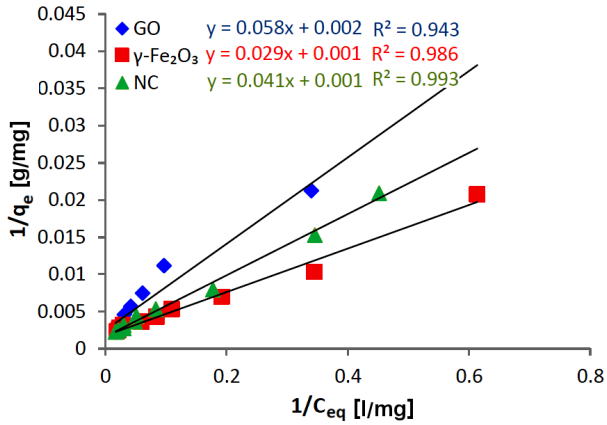

Figure 12. Langmuir adsorption isotherms for Ni(II) ions adsorption using GO, γ-Fe_2O_3 and NC at 25 °C

and 99.9% was observed for GO, γ-Fe_2O_3 and NC, respectively and it was decreased down to 87.2%, 89.5% and 91.7%, respectively, when solution concentration was increased to 500 mg/l. These findings are attributed to the increase in the number of ions available at higher concentration which compete for the available sorption sites. Accordingly, this is connected with the lack of binding sites on the adsorbents itself.

3.7. Adsorption isotherm studies

Adsorption isotherms were also studied to investigate the adsorption capacity of synthesized adsorbents for Ni(II) ions. The parameters computed from adsorption isotherms are listed in Table 4. Maximum adsorption capacity (q_{max}) calculated from Langmuir adsorption isotherms was 403.7, 572.4 and 615.0 mg/g for GO, γ-Fe_2O_3 NPs and NC, respectively (Fig. 12). The monolayer adsorption capacities of the adsorbents used in the present studies for the removal of Ni(II) ions have been compared with other adsorbents synthesized by various researchers and reported in Table 5. The value of q_{max} for synthesized NC is higher than all other adsorbents reported earlier. The Freundlich plots (Fig. 13) depicted that the value of n for GO, γ-Fe_2O_3 NPs and NC was 1.27, 1.67 and 1.77, respectively, and this indicates favourable adsorption process. The adsorption capacity was the highest for NC followed by γ-Fe_2O_3 NPs and GO as confirmed by the Freundlich constants (K_f): 49.54, 41.97 and 16.82 mg/l respectively. D-R isotherms were used to calculate the values of D-R constant β (coefficient associated with energy) and q_{max}. The calculated values of mean sorption energy (E) were less than 1 kJ/mol and this signifies the physical nature of adsorption process. However, D-R model is not followed perfectly as clearly indicated by regression coefficient (R^2) values ranged from 0.59 to 0.86. Temkin isotherms

Table 5. Langmuir adsorption capacity (q_{max}) of various adsorbents for Ni(II) ions

Adsorbent	q_{max} [mg/g]	Optimum pH	Reference
Powder babhul bark	5.90	8.0	[43]
Powder activated charcoal	6.70	8.0	[43]
Graphene oxide/saw dust composite	135.50	10.0	[20]
Iron oxide NPs	0.23	10.0	[48]
NaOH-Modified coconut husk	73.52	8.0	[49]
Activated Carbon	-	8.0	[50]
GO	403.70	10.0	This study
NC	615.00	10.0	This study
γ-Fe_2O_3	572.40	10.0	This study

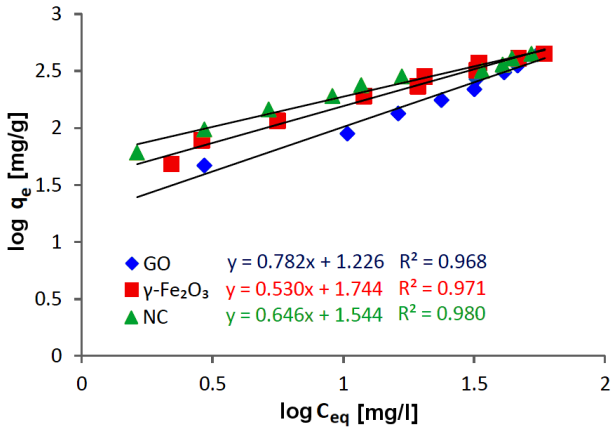

Figure 13. Freundlich adsorption isotherms for Ni(II) ions adsorption using GO, γ-Fe_2O_3 and NC at 25 °C

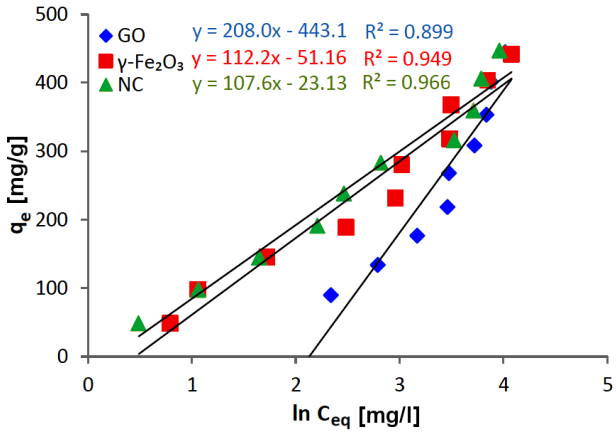

Figure 14. Temkin isotherms for Ni(II) ions adsorption

mentioned in Fig. 14 revealed that value of Temkin binding constant (A) varied from 0.11 to 0.80 l/g being maximum in NC which signifies higher binding capacity of adsorbent. The value of parameter B ranged from 107.6 to 208.0 J/mol which further confirmed the heat of sorption and physical adsorption process.

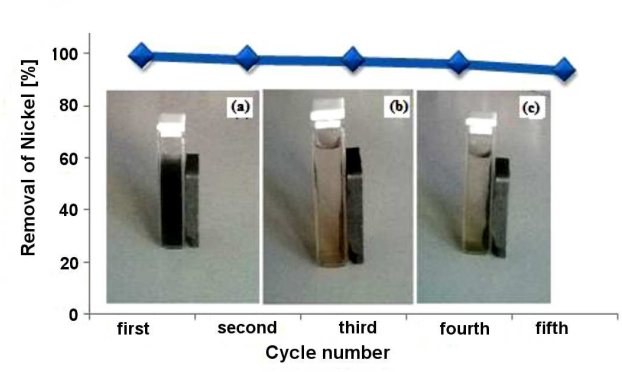

Figure 15. Removal of Ni(II) ions by NC after five adsorption/desorption cycles (inset image shows magnetic separation of a) GO b) γ-Fe_2O_3 and c) NC by magnet

3.8. Regeneration studies

The main aim of regeneration studies is to remove and reuse the spent adsorbent. The synthesized γ-Fe_2O_3-GO NC could be easily separated from the solution with the help of an ordinary magnet (inset of Fig. 15).The desorption cannot be performed on γ-Fe_2O_3 as they get easily dissolved in acidic solution [47]. γ-Fe_2O_3 NPs immobilized on GO offers not only simple method of magnetic separation but also inhibits γ-Fe_2O_3 acid dissolution on regeneration. The use of 0.01 M HCl was the best treatment for removal of adsorbed Ni(II) ions. Removal efficiency of regenerated NC after successive cycles is presented in Fig. 15 and it was 95% even after five adsorption-desorption cycles.

IV. Conclusions

In the present studies, environmentally stable magnetic nanocomposite was synthesized by facile sonication method. Structural characterization using Mössbauer spectrometry confirmed the presence of γ-Fe_2O_3 along with GO in the nanocomposite and absence of any mixed Fe^{2+}–Fe^{3+} phase. The sorption capacity of nanocomposite for Ni(II) ions was higher than GO, γ-Fe_2O_3 and other adsorbents reported earlier in the literature. Increase in the adsorption potential of γ-Fe_2O_3–GO (NC) is due to the immobilization of γ-Fe_2O_3 on GO which favoured the process of adsorption. NC is insoluble in water, easily separated by magnet and can be effectively reused after regeneration. It has an immense potential as an absorbent for the removal of Ni(II) ions from the aqueous solution and can be explored as an effective adsorbent for the remediation of other pollutants.

References

1. M. Rao, A.V. Parwate, A.G. Bhole, “Uptake of nickel from aqueous solution using low cost adsorbent”, *Poll. Res.*, **20** (2001) 669–675.
2. R.C. Bansal, M. Goyal, *Activated Carbon Adsorption*, CRC Press, New York, 2005.
3. C.C. George, *Electroplating Wastewater Pollution Control Technology*, Park Ridge, Noyes Publications, 1985.
4. K.H. Chong, B. Volesky, “Description of two-metal biosorption equilibria by Langmuir-type models”, *Biotech. Bio. Eng.*, **47** (1995) 451–460.
5. A. Mittal, J. Mittal, A. Malviya, D. Kaur, V.K. Gupta, “Decoloration treatment of a hazardous triarylmethane dye, Light Green SF (Yellowish) by waste material adsorbents”, *J. Colloid Interf. Sci.*, **342** (2010) 518–527.
6. V.K. Gupta, I. Ali, T.A. Saleh, A. Nayak, S. Agarwal, “Chemical treatment technologies for waste-water recycling - An overview”, *RSC Adv.*, **2** (2012) 6380–6388.
7. A. Akbarzadeh, M. Samiei, S. Davaran, “Magnetic nanoparticles: Preparation, physical properties, and applications in biomedicine”, *Nanoscale Res. Lett.*, **7** (2012) 1–14.
8. R.M. Cornell, H.C.U. Schwertmann, *The Iron Oxides: Structures, Properties, Reactions, Occurrences and Uses*,

Wiley-VCH, Weinheim, 2003.
9. A.K. Geim, K.S. Novoselov, "The rise of graphene", *Nat. Mater.*, **6** (2014) 183–191.
10. A.K. Geim, "Graphene: Status and prospects", *Science*, **324** (2009) 1530–1534.
11. K.S. Novoselov, A.K. Geim, S.V. Morozov, D. Jiang, Y. Zhang, S.V. Dubonos, I.V. Grigorieva, A. Firsova, "Electric field effect in atomically thin carbon films", *Science*, **306** (2014) 666–669.
12. G.D. Sheng, Y.M. Li, H.P. Dong, D.D. Shao, "Environmental condition effects on radionuclide ^{64}Cu(II) sequestration to a novel composite: Polyaniline grafted multiwalled carbon nanotubes", *J. Radioanal. Nucl. Chem.*, **293** (2012) 797–806.
13. G.X. Zhao, J.X. Li, X.M. Ren, C.L. Chen, X.K. Wang, "Few-layered graphene oxide nanosheets as superior sorbents for heavy metal ion pollution management", *Environ. Sci. Technol.*, **45** (2011) 10454–10462.
14. C. Xu, A. Cui, Y. Xu, X. Fu, "Graphene oxide-TiO_2 composite filtration membranes and their potential application for water purification", *Carbon*, **62** (2013) 465–471.
15. Y. Gao, Y. Li, L. Zhang, H. Huang, H. Junjie, S. Shah, X. Su, "Adsorption and removal of tetracycline antibiotics from aqueous solution by graphene oxide", *J. Colloid Interf. Sci.*, **368** (2012) 540–546.
16. F. Najafi, O. Moradi, M. Rajabi, M. Asif, I. Tyagi, S. Agarwal, V.K. Gupta, "Thermodynamics of the adsorption of nickel ions from aqueous phase using graphene oxide and glycine functionalized graphene oxide", *J. Mol. Liq.*, **208** (2015) 106–113.
17. S. Luo, X. Xu, G. Zhou, C. Liu, Y. Tang, Y. Liu, "Amino siloxane oligomer-linked graphene oxide as an efficient adsorbent for removal of Pb(II) from wastewater", *J. Hazard. Mater.*, **274** (2014) 145–155.
18. F. Fang, L. Kong, J. Huang, S. Wu, K. Zhang, X. Wang, B. Sun, Z. Jin, J. Wang, X.J. Huang, J. Liu, "Removal of cobalt ions from aqueous solution by an amination graphene oxide nanocomposite", *J. Hazard. Mater.*, **270** (2014) 1–10.
19. V.K. Gupta, S. Agarwal, H. Sadegh, G.A.M. Ali, A.K. Bharti, A.S.H. Makhlouf, "Facile route synthesis of novel graphene oxide-β-cyclodextrin nanocomposite and its application as adsorbent for removal of toxic bisphenol A from the aqueous phase", *J. Mol. Liq.*, **237** (2017) 466–472.
20. Y. Wu, H. Luo, H. Wang, L. Zhang, P. Liu, L. Feng, "Fast adsorption of nickel ions by porous graphene oxide/sawdust composite and reuse for phenol degradation from aqueous solution", *J. Colloid Interf. Sci.*, **436** (2014) 90–98.
21. J.H. Deng, X.R. Zhang, G.M. Zeng, J.L. Gong, Q.Y. Niu, J. Liang, "Simultaneous removal of Cd(II) and ionic dyes from aqueous solution using magnetic graphene oxide nanocomposite as an adsorbent", *Chem. Eng. J.*, **226** (2013) 189–200.
22. Y. Fu, J. Wang, Q. Liu, H. Zeng, "Water-dispersible magnetic nanoparticle-graphene oxide composites for selenium removal", *Carbon*, **77** (2014) 710–721.
23. Y. Guo, J. Deng, J. Zhu, X. Zhou, R. Bai, "Removal of mercury(II) and methylene blue from of wastewater environment with magnetic graphene oxide: adsorption kinetics, isotherms and mechanism", *RSC Advance*, **6** (2006) 82523–82536.
24. X.J. Hu, Y. G. Liu, H. Wang, G. Zeng, X. Hu, Y. Guo, T. Li, A. Chen, L. Jiang, F. Guo, "Adsorption of copper by magnetic graphene oxide-supported cyclodextrin: Effects of pH, ionic strength, background electrolytes, and citric acid", *Chem. Eng. Res. Des.*, **93** (2015) 675–683.
25. K. Zhang, V. Dwivedi, C. Chi, J. Wu, "Graphene oxide/ferric hydroxide composites for efficient arsenate removal from drinking water", *J. Hazard. Mater.*, **182** (2010) 162–168.
26. V. Chandra, J. Park, Y. Chun, J.W. Lee, I.C. Hwang, K.S. Kim, "Water-dispersible magnetite-reduced graphene oxide composites for arsenic removal", *ACS Nano*, **4** (2010) 3979–3986.
27. M. Liu, C. Chen, J. Hu, X. Wu, X. Wang, "Synthesis of magnetite/graphene oxide composite and application for cobalt (II) removal", *J. Phys. Chem. C.*, **115** (2011) 25234–25240
28. M. Kaur, M. Singh, S.S. Mukhopadhyay, D. Singh, M. Gupta, "Structural, magnetic and adsorptive properties of clay ferrite nanocomposite and its use for effective removal of Cr (VI) from water", *J. Alloy. Compd.*, **653** (2015) 202–211.
29. H. Wang, X. Yuab, Y. Wu, H. Huang, G. Zeng, Y. Liu, X. Wang, N. Lin, Y. Qi, "Adsorption characteristics and behaviors of graphene oxide for Zn(II) removal from aqueous solution", *Appl. Surf. Sci.*, **279** (2013) 432–440.
30. Z. Marczenko, *Separation and Spectrophotometric Determination of Elements*, 4th ed., John Wiley and Sons Company. Inc., England, 1976.
31. M.E. Batouti, A.M. Ahmed, "Adsorption kinetics of nickel (II) onto activated carbon prepared from natural adsorbent rice husk", *Int. J. Technol. Enhanc. Merg. Eng. Res.*, **2** (2014) 2347–4289.
32. H. Wang, X. Yuan, Y. Wu, H. Huang, X. Peng, G. Zeng, H. Zhong, J. Liang, M. Ren, "Graphene-based materials: fabrication, characterization and application for the decontamination of wastewater and waste gas and the hydrogen storage/generation", *Adv. Colloid. Interfac.*, **195** (2013) 19–40.
33. L.Z. Bai, D.L. Zhao, Y. Xu, J.M. Zhang, Y.L. Gao, L.Y. Zhao, J.T. Tang, "Inductive heating property of graphene oxide-Fe_3O_4 nanoparticles hybrid in an AC magnetic field for localized hyperthermia", *Mater. Lett.*, **68** (2012) 399–401.
34. M.A. Abdalla, M.H. Jaafar, Z.A. Al-Othman, S.M. Alfadul, M. Ali Khan, "New route for preparation and characterization of magnetite nanoparticles", *Arab. J. Chem.*, **4** (2011) 235–237.
35. C.C. Huang, H.S. Li, C.H. Chen, "Effect of surface acidic oxides of activated carbon on adsorption of ammonia", *J. Hazard. Mater.*, **159** (2008) 523–527.
36. G. Svehla, *Textbook of Macro and Semi Micro Qualitative Inorganic Analysis*, Fifth ed., Longman Inc., New York, USA, 1979.
37. F.Y. Ban, S.R. Majid, N.M. Huang, H.N. Lim, "Graphene oxide and its electrochemical performance", *Int. J. Electrochem. Sci.*, **7** (2012) 4345–4351.
38. J.L. Gong, B. Wang, G.M. Zeng, C.P. Yang, C.G. Niu, Q.Y. Niu, W.J. Zhou, Y. Liang, "Removal of cationic dyes from aqueous solution using magnetic multi-wall carbon nanotube nanocomposite as adsorbent", *J. Hazard. Mater.*, **164** (2009) 1517–1522.
39. A. Jaiswal, S. Banerjee, R. Mani, M.C. Chattopadhyaya,

"Synthesis, characterization and application of goethite mineral as an adsorbent", *J. Environ. Chem. Eng.*, **1** (2013) 281–289.

40. X. Yang, C. Chen, J. Li, G. Zhao, X. Ren, X. Wang, "Graphene oxide-iron oxide and reduced graphene oxide-iron oxide hybrid materials for the removal of organic and inorganic pollutants", *RSC. Adv.*, **2** (2012) 8821–8826.
41. L. Shahriary, A. Athawale, "Graphene oxide synthesized by using modified Hummers approach", *Int. J. Renew. Energy. Environ. Eng.*, **2** (2014) 1–6.
42. J. Hur, J. Shin, J. Yoo, Y.S. Seo, "Comparative adsorption of metals onto magnetic graphene oxide: Comparison with carbonaceous adsorbents",*Scientific World J.*, **2015** (2015) 1–11.
43. S.J. Patil, A.G. Bhole, G.S. Natarjan, "Scavenging of Ni(II) metal ions by adsorption on PAC and babhul Bark", *J. Environ. Sci. Eng.*, **48** (2006) 203–208.
44. N. Kawasaki, R. Bunei, F. Ogata, S. Tanei, S. Tanada, "Water treatment technology using carbonaceous materials produced from vegetable biomass", *J. Water Environ. Technol.*, **4** (2006) 73–82.
45. P. Saha, S. Chowdhury, *Insight Into Adsorption Thermodynamics*, InTech, 2011.
46. J. Wang, S. Zheng, Y. Shao, J. Liu, Z. Xu, D. Zhu, "Amino-functionalized Fe_3O_4@SiO_2 core-shell magnetic nanomaterial as a novel adsorbent for aqueous heavy metals removal", *J. Colloid. Interface. Sci.*, **349** (2010) 293–299.
47. M.H. Salmani, M.H. Ehrampoush, M.A. Jahromi, M. Askarishahi, "Comparison between Ag (I) and Ni (II) removal from synthetic nuclear power plant coolant water by iron oxide nanoparticles", *J. Environ. Health Sci. Eng.*, **11** (2013) 1–7.
48. O.K. Olayinka, O.A. Oyedeji, O.A. Oyeyiola, "Removal of chromium and nickel ions from aqueous solution by adsorption on modified coconut husk", *J. Environ. Sci. Technol.*, **3** (2009) 286–293.